Behaviour of Cold-Formed Steel-Concrete Composite Columns under Axial Compression: Experimental and Numerical Study

Senthilkumar Rajendran[1], Divya Mohan[1], Divya Roy S[1], Bahurudeen Abdul Salam[2], Siva Avudaiappan[3] and Konstantinos Daniel Tsavdaridis[4]

[1]Department of Civil Engineering, National Institute of Technology Tiruchirappalli, Tiruchirappalli, Tamil Nadu, India
[2]Department of Civil Engineering, BITS – Pilani Hyderabad Campus, Hyderabad, India.
[3]Departamento de Ingeniería en Obras Civiles, Universidad de Santiago de Chile, Av. Ecuador 3659, Estación Central, Chile
[4]Department of Civil Engineering, School of Mathematics, Computer Science and Engineering, City, University of London, Northampton Square, EC1V 0HB, London, UK

*****Correspondence: Senthilkumar Rajendran senthilr@nitt.edu *

Abstract: Concrete filled cold-formed steel-concrete composite columns exhibit improved strength and ductility characteristics due to its ability to resist inward buckling as well as delay the outward buckling. Though concrete infill prevents inward buckling, outward buckling still limits the steel section from reaching its yield strength. From the past studies, it is observed that the introducing of web stiffeners in cross-section of steel section may improve its buckling resistance. The present study focuses on assessing the effect of longitudinal stiffeners on the behaviour of square cold-formed steel-concrete composite columns for the various slenderness range (0.01 to 0.4) through experimental and numerical studies. Conventionally, the integrity of hollow tube cross sections is ensured by welding or by rolling process during the manufacturing. Welding process cannot be adopted in thin-walled cold formed sections since it may lead to higher degree of imperfection. In this study, the desired square cross sections were formed from flat steel sheet and overlapped using self-tapping screws. An intensive numerical analysis was carried out by varying stiffener angle as 90^0, 120^0, and 141^0 and the buckling curves for plain and profiled sections were presented. It is concluded that the axial compressive strength of plain and stiffened composite sections is almost equal, attributed to the inability of concrete to reach its maximum stress due to stress concentration at the stiffeners' edges. The buckling reduction factor of stiffened composite columns showed higher values in the higher slenderness range, indicating the positive effect of the stiffeners.

Keywords: Composite Columns; Cold-formed steel; Stiffeners; Local Buckling; Experimental tests; Nonlinear FE Analysis

1. Introduction

The extensive use of thin-walled members in constructional industries is mostly due to their high strength-to-weight attributes and superior fabrication versatility. Primarily, hot-rolled steel sections are used for steel-concrete composite structures [1]. However, nowadays cold-formed sections are begin to replace the hot-rolled sections due to their inherent advantages [2]. The composite columns especially hot rolled sections are made by two techniques, one is encased steel section, and the other is Concrete-Filled Steel Tubular (CFST) section. When comparing these two techniques, the confinement effect in CFST section has proven beneficial to withstand larger gravitational loads than its counterpart [3]. Rahnavard et al. (2022) have studied the behaviour column at four different cross sectional shapes and found that steel component withstands higher compressive strength when it is used in composite column than bare steel column.[4] Evirgen et al, 2014 [5] have studied the behaviour of column with various cross-sectional shapes like Circular, hexagonal, rectangular and square sections and found that circular section outstands all. The major limitation of square and rectangular concrete filled composite sections is its inability to withstand the outward buckling of steel tubes [6], [7] which was witnessed in cold formed composite columns also [8]. Ge & Usami, 1994 have increased the performance of square and rectangular column by adopting different stiffening schemes[9]. Huang et al. (2002) proposed a set of

four steel bars at regular spacing along the tube axis and it found to increase both strength and ductility[10].

Tao et al (2005) presented the improvement of ductile behaviour of stiffened composite stub columns with various methods as shown in fig.1. [11] Their research showed that although all different stiffening methods have potentials to improve the ductility of the stiffened stub columns to some extent, adding fibres to concrete is the most effective and reliable measurement in increasing the ductility capacity.

Nassirnia et al. (2015) studied the effect of corrugation in delaying the local buckling of hollow columns, and it exhibited better compressive strength and energy dissipation It was found that the ductility increases with the number or width of inner stiffeners.[12]

Usually, in hot rolled members stiffeners can be directly welded to the section. However, such practice is not feasible for thin-walled section as it may lead to generation of residual stresses and geometrical imperfection. Hence stiffening can be achieved by corrugating the flat sheet. The corrugation shape provides continuous stiffening which permits the use of thin sheets. A corrugated sheets can easily be bent in one direction, whereas it retains its rigidity in the other direction. Fabrication costs for elements with corrugated panels are normally lower than those elements with additional stiffeners.

Thus, the present study aims to evaluate the effectiveness of corrugations as web stiffener in the load-carrying capacities of cold formed steel hollow column and cold formed steel concrete composite column. The square cross section was adopted since it would be difficult to make circular section in cold formed steel. The square columns were tested for two conditions with and without stiffeners (ie) column made of flat and corrugated flat sheet respectively. A parametrical study was also carried out by adopting various changes in corrugation. The flat sheets were bent and formed as square section using self-tapping screws. In this study, specimens were tested for with and without stiffener condition in three different slenderness range. Numerical studies were done for various stiffeners and appropriate buckling curve for various slenderness range were presented.

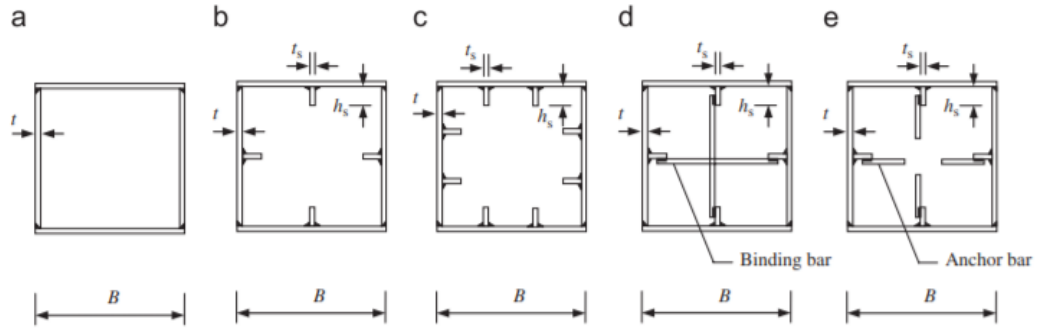

(a) Unstiffened Specimens (b) stiffened specimen with one stiffener on each face (c) stiffened specimen with two stiffeners on each face (d) stiffened specimen with binding bars and (c) stiffened specimens with anchor bars

Fig. 1. Stiffening schemes proposed by Tao et al[13]

2. Experimental Study

2.1 General

An experimental program comprising 36 specimens was undertaken to determine the concentric axial load carrying capacity of square cold-formed plain steel columns (without stiffeners), cold-formed steel profiled columns (with web stiffeners), cold-formed steel plain composite columns, and cold-formed profiled composite columns. The effectiveness of an under-investigated connection system using self-tapping screws is also evaluated in this study.

2.2 Test Specimens

The column dimension adopted for the experimental study was 100mm x 100mm. The columns were tested for two different systems – with and without stiffeners. The stiffeners were introduced in the form of intermediate bends in the cross-section as the most appropriate method to stiffen Cold formed sections. Three different slenderness were selected to study the complete behaviour of the column. The nomenclature adopted is presented in Table 1. The first letter in the nomenclature S, I, L stands for Short, Intermediate and Long columns. The letters that follow, NP stands for non-Profiled sections, and

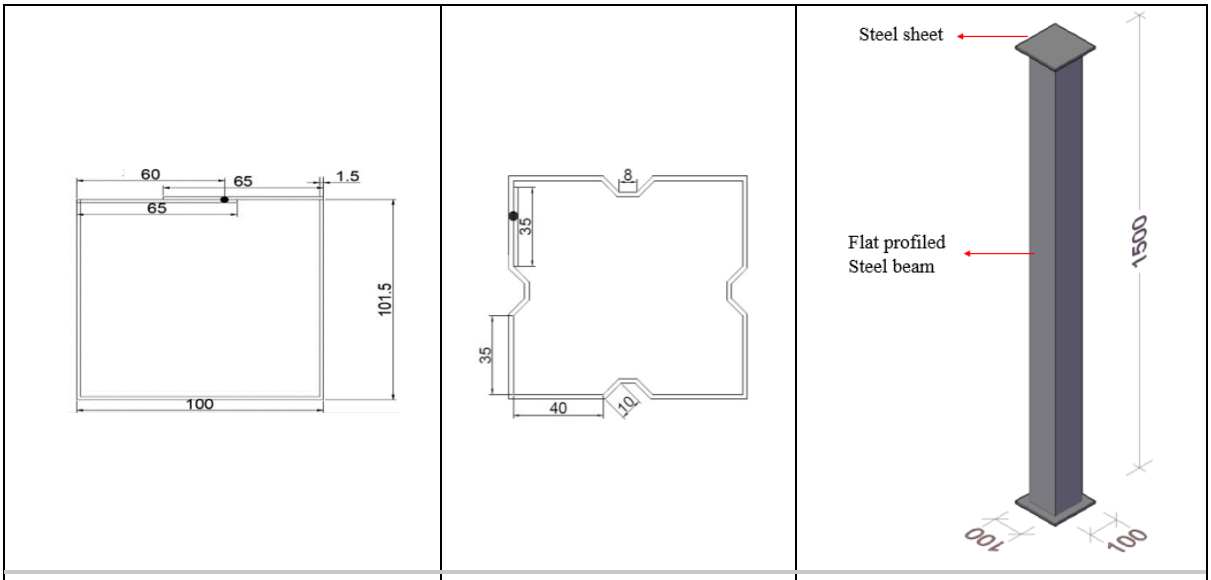

(a) Plain Section | (b) Profiled Section | (c) Elevation of specimen

All dimensions are in mm

Fig. 2 Cross-section details of the specimens

P stands for Profiled sections. The letter S at the end of nomenclature stands for Steel only column, and C stances for Composite column. The cross-sectional dimensions of the plain and profiled specimens are shown in Fig. 2.

Table 1: Details of the specimen

	Hollow						**Composite**					
Type	**Plain**			**Profiled**			**Plain**			**Profiled**		
Length (mm)	500	1500	2000	500	1500	2000	500	1500	2000	500	1500	2000
Nomenclature	SNPS	INPS	LNPS	SPS	IPS	LPS	SNPC	INPC	LNPC	SPC	IPC	LPC
KL/r	12.62	37.86	50.48	12.84	38.52	51.36	15.30	45.90	61.20	15.35	46.04	61.39
λ	0.011	0.032	0.042	0.012	0.034	0.044	0.022	0.193	0.344	0.026	0.229	0.387

2.3 Materials

2.3.1 Cold-Formed Steel

CFS steel of 1.6 mm thickness was used for the fabrication of the specimens. Coupons of dimensions complying with the ASTM Standards in Building Code [14] were extracted from the steel plate. The tensile coupon test specimens were extracted by the wire-cut electrode discharge machining (EDM). In this method there is no physical stress applied on the material and it does not produce any feed marks on it. The material is disintegrated by the spark generated from electrically charged molybdenum wire. This disintegrated material is further cooled and flushed by a dielectric fluid. This phenomenon happens over thousands of times per second [15]. The tensile coupon tests were conducted to record the yield and ultimate stresses and the modulus of the elasticity. The average values gained from the test are listed in Table 2.

Table 2: Coupon Test Results

Parameter	**Value**
Yield Stress	165 MPa
Ultimate Stress	304 MPa
Young's Modulus	$2.1*10^5$ MPa

2.3.2 Concrete

Self-compacting concrete was adopted to ease the process of concrete placement and to avoid irregularities. The mix design that gives the desired strength of 30 MPa was achieved after the three trials (9 specimens) as per IS 516 [16] and IS 10262 [17] standards. The cube specimens were tested statically after seven days to confirm concrete strength, and the rest were tested after 28 days of curing. The details of the tests are tabulated in Table 3. The difference between the results can be due to workmanship and material quality.

Table 3: Compressive Strength Test of Concrete

S. No.	**Cube Strength (MPa)**	
	7^{th} day	**28^{th} day**
1.	22.8	36
2.	29.6	37.8
3.	34.6	34.5

2.4 Connection

In general, welding is not desirable when the thickness of the plate is less than 3mm [18], as it creates imperfections and may even lead to the melting of plates. Hence, a novel system of connection using self-tapping screws is introduced to avoid welding. The self-tapping screws can be easily drilled into plates of lesser thickness, while it holds the plates together through the groves made by it when it is drilled. The dimension of the screw was 5mm diameter and 45mm in length. The screws capacity was assessed by a single lap shear test, as shown in Fig. 3, and its behaviour is shown in Fig. 5. From the Single lap shear test, the ultimate capacity of the screw is found to be 6.9kN. The adopted spacing also ensures that the connections do not fail before the specimens yield and satisfying the minimum edge distance conditions.

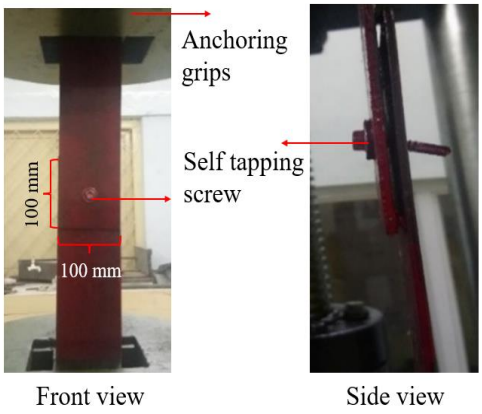

Fig. 3 Testing of self-tapping screws

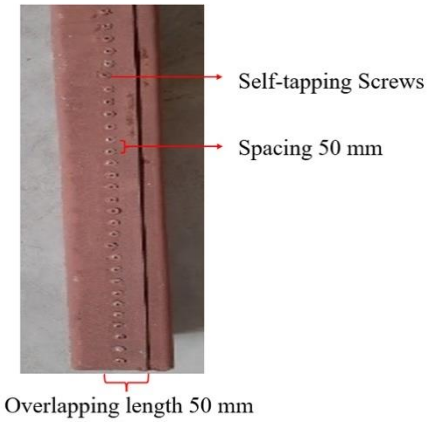

Fig. 4 Hollow column with self-tapping screw

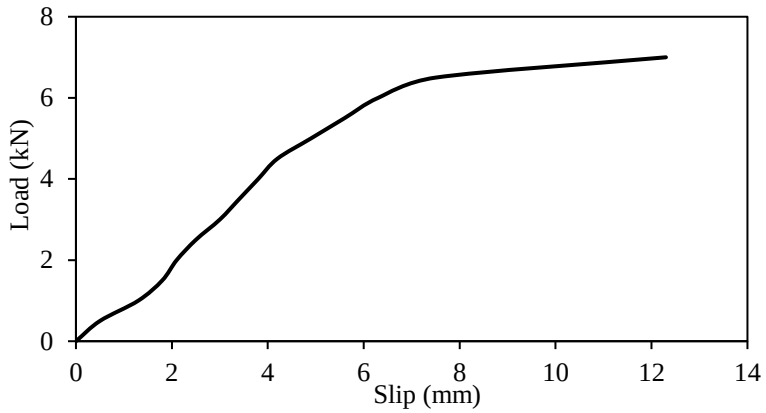

Fig. 5 Load-Displacement Curve of Self-Tapping Screw

2.5 Specimen Preparation

The encasing steel tubes were cold formed into the desired shape, overlapped and connected with self-tapping screws. For the composite specimens, SCC concrete was poured into the steel tubes. The concrete was filled in three or four layers (depending on the sample's height), manually compacted with a tamping rod. Each concrete layer was prepared with at least twenty-five strokes. The upper surface was levelled, and the samples were kept aside for curing for 28 days.

2.6 Experimental Set-up

A hydraulic pump was used to apply the axial load on the specimens. The support conditions assumed were pinned, and it was achieved by providing two hinged plates on both sides of the column. The behavioural responses of the specimens were recorded using dial gauges. Fig. 6 shows the experimental setup.

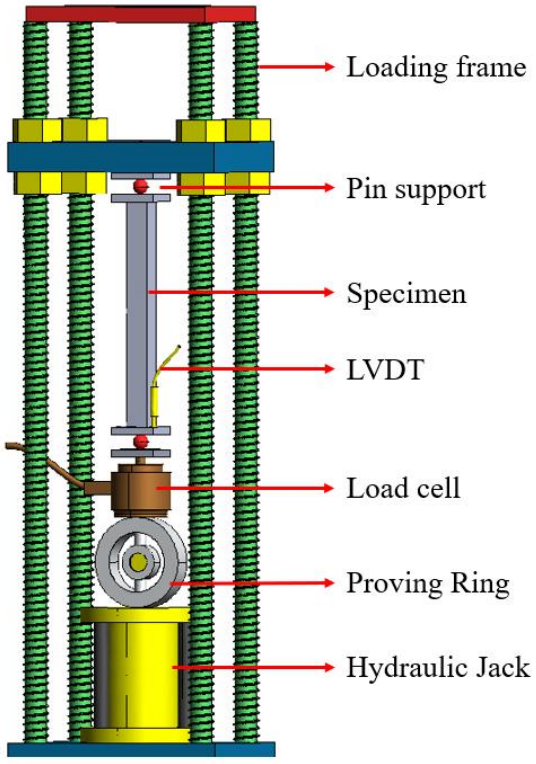

Fig. 6 Test set-up for axial compression test of columns

2.7 Results and Discussion

2.7.1 Failure Behaviour

From the experimental investigations, it was found that all plain hollow sections (SNPS, INPS and LNPS) failed by local buckling, SPS failed by local buckling while global buckling was initiated in the case of IPS and LPS sections [19]. The provision of stiffeners increased the load carrying capacity of hollow columns remarkably by 23.3%, 21.3%, and 19.9 % in short, intermediate, and long columns, respectively.

The prominent mode of failure observed in the case of composite columns was the crushing of concrete. Crushing of concrete was found to limit the column strength in the case of profiled composite columns compared to the plain composite columns. The self-tapping screws remained intact till the failure of columns and hence it can be considered that they provide a rigid connection.

3. Analytical Studies

Design philosophies proposed by some of the prominent codes are used to estimate the axial strength of the test specimens.

3.1 Hollow Columns

BS 5950-5:1998 [20] and AISI S100-16 [21] code provisions are used to determine the axial strength of hollow columns.

3.1.1 BS 5950-5:1998

For sections symmetrical about both principal axes or closed cross-sections which are not subject to torsional flexural buckling, or braced against twisting, the buckling resistance under axial load, P_c, may be obtained from the following:

$$P_c = \frac{(P_e P_{cs})}{(\phi + \sqrt{((\phi^2) - P_e P_{cs})}} \quad (1)$$

where $\phi = \frac{P_{cs} + (1+\eta) P_e}{2}$,

P_{cs} is the short strut capacity $P_{CS} = A_{eff} \times P_y$

A_{eff} is the effective cross-sectional area; P_y is the design strength; P_e is the minimum elastic flexural buckling load $P_e = \frac{\pi^2 EI}{L^2}$, E is the modulus of elasticity; I is the moment of inertia of the cross-section about the critical axis; L_e is the effective length of the member about the critical axis; η is the Perry coefficient, such that:

for $\frac{L_e}{r} \leq 20$, $\eta = 0$

for $\frac{L_e}{r} > 20$, $\eta = 0.002(\frac{L_e}{r} - 20)$

where r is the radius of gyration of the gross cross-section corresponding to P_e.

The effects of local buckling should be considered in determination of the design strength and stiffness of cold formed members. This may be accomplished using effective cross-sectional properties which are calculated on the basis of the widths of individual elements.

In the case of elements which are adequately supported on both longitudinal edges, i.e., stiffened elements, the effective width of the element should be taken as composed of two equal portions, one adjacent to each edge.

for $\frac{f_c}{P_{cr}} \leq 0.123$

$\frac{b_{eff}}{b} = 1$

for $\frac{f_c}{P_{cr}} > 0.123$

$$\frac{beff}{b} = \left[1 + 14\left\{\left(\frac{f_c}{P_{cr}}\right)\frac{1}{2} - 0.35\right\}\right] - 0.2 \quad (2)$$

where f_c is the compressive stress on the effective element; p_{cr} is the local buckling stress of the element given by:

$$P_{cr} = 0.904EK\left(\frac{t}{b}\right)^2 \quad (3)$$

where K is the local buckling coefficient which depends on element type, section geometry t is the material thickness. The effective cross-sectional area, A_{eff} is computed from b_{eff}.

3.1.2 AISI S100-16

For the effective width method, the nominal axial strength (resistance), P_{nl}, for local buckling shall be calculated in accordance with the following:

$$P_{nl} = A_e \times F_n \leq P_{ne} \quad (4)$$

where F_n is the global column stress, A_e is the effective area calculated at stress F_n, P_{ne} is the nominal strength considering yielding and global buckling.

By the strength determination criteria, the effective width, b, shall be calculated as follows:

$$b = \rho \times w \tag{5}$$

where w is the flat width, ρ is the local reduction factor:

$\rho = 1$ when $\lambda \leq 0.673$

$\rho = \frac{(1-0.22/\lambda)}{\lambda}$ when $\lambda > 0.673$

where λ is the slenderness factor $\lambda = \sqrt{\frac{f}{F_{crl}}}$, f is the compressive stress in element considered, F_{crl} is the minimum critical buckling stress of the cross-section:

$$F_{crl} = k \frac{\pi^2 E}{12(1-\mu^2)} (\frac{t}{w})^2 \tag{6}$$

where k is the plate buckling coefficient, $k = 4$ for stiffened elements supported by a web on each longitudinal edge. E is the modulus of elasticity of steel, t is the thickness of uniformly compressed stiffened element, μ is the Poisson's ratio of steel.

The nominal axial strength, P_{ne}, for yielding and global (flexural, torsional and flexural-torsional) buckling is computed as follows:

$$P_{ne} = A_g F_n \tag{7}$$

where A_g is the gross area, F_n is the compressive stress:

$F_n = \left(0.658^{\lambda_c{}^2}\right) F_y$ *for* $\lambda_c \leq 1.5$

$F_n = \left(\frac{0.877}{\lambda_c{}^2}\right) F_y$ *for* $\lambda_c > 1.5$

where $\lambda_c = \frac{F_y}{F_{cre}}$, F_y is the yield stress, F_{cre} is the least of the applicable elastic global (flexural, torsional and flexural-torsional buckling) stresses:

$$F_{cre} = \frac{\pi^2 E}{\left(\frac{KL}{r}\right)^2} \tag{8}$$

For a concentrically loaded compression member with a closed-box section that is made of steel with a specified minimum elongation between three to ten percent, inclusive, a reduced radius of gyration $(R_r)*r$ shall be used when the value of the effective length KL is less than $1.1*L_o$.

where L_0 is the length at which local buckling stress equals flexural buckling stress:

$$L_0 = \pi r \sqrt{\frac{E}{F_{crl}}} \tag{9}$$

where r is the radius of gyration of unreduced cross-section about axis of buckling R_r is the reduction factor:

$$R_r = 0.65 + \frac{0.35KL}{1.1L_0} \tag{10}$$

For the profiled sections, the area of cross-section and second moment of area is modified accordingly. The results obtained are tabulated in Table 4. It is found that both code provisions are in good agreement with the experimental test results. BS 5950 is more compatible with the experimental results than AISI. It states that the self-tapping screw connection can be used to make cold-formed steel tubular sections to utilise the full capacity.

Table 4: Comparison of experimental and analytical results of hollow columns

Specimen	**KL/r**	**λ**	**Test (kN)**	**BS 5950-5 (kN)**	**AISI S100-16 (kN)**	**Test/ BS 5950-5**	**Test/AISI S100-16**
SNPS	12.62	0.011	90.8	85.1	82.8	1.07	1.10
INPS	37.86	0.032	86.2	81.9	78.7	1.05	1.09
LNPS	50.48	0.042	84.6	79.4	76.16	1.06	1.11
SPS	12.84	0.012	112.3	105.6	105.0	1.06	1.07
IPS	38.52	0.034	104.6	101.6	97.2	1.03	1.08
LPS	51.36	0.044	101.5	98.3	92.6	1.03	1.06
Mean						1.05	1.085
SD						0.017	0.019
CV%						1.59	1.72
β						2.94	3.08
λ is non-Dimensional slenderness ratio, KL/r is Effective Slenderness ratio, β is the reliability index, CV% is the coefficient of variation in percentage, SD is the Standard Deviation.							

3.2 Composite Columns

The existing design codes do not incorporate any design guidelines for cold-formed steel composite columns, neither for axial nor for eccentric loading. Hence, design guidelines about hot-rolled steel-concrete composite columns are employed herein to calculate the approximate axial strength for columns with cold-formed steel. The existing codes account only for the section with a higher thickness that does not undergo any local buckling. [22]They consider only the nominal compressive strength of the sections. The design codes based on composite columns used in the present study are AISC 360-16 [32] and EC4 [30].

3.2.1 AISC 360-16

The design compressive strength, P_n of doubly symmetric axially loaded encased composite members shall be determined for the limit state of flexural buckling based on member slenderness as follows:

For $\frac{P_{no}}{P_e} \leq 2.25$

$$P_n = P_{no}\left(0.658^{\frac{P_{no}}{P_e}}\right) \quad (11)$$

For $\frac{P_{no}}{P_e} > 2.25$

$$P_n = 0.877P_e \quad (12)$$

$$P_{no} = F_y A_s + F_{ysr} A_{sr} + 0.85 f_c' A_c \quad (13)$$

where P_e is the elastic buckling load.

$P_e = \frac{\pi^2 (EI_{eff})}{{L_c}^2}$, A_c is the area of concrete, A_s is the cross-sectional area of steel section, E_c is the modulus of elasticity of concrete, EI_{eff} is the effective stiffness of composite section:

$$EI_{eff} = E_s I_s + E_s I_{sr} + C_1 E_c I_c \quad (14)$$

C_1 = coefficient for calculation of effective rigidity of an infilled composite compression member:

$$C_1 = 0.25 + 3\left(\frac{A_s + A_{sr}}{A_g}\right) \leq 0.7 \quad (15)$$

E_s is the modulus of elasticity of steel, F_y is the specified minimum yield stress of steel section, F_{ysr} is the specified minimum yield stress of reinforcing bars, I_c is the moment of inertia of the concrete section about the elastic neutral axis of the composite section, I_s is the moment of inertia of steel shape about the elastic neutral axis of the composite section, I_{sr} is the moment of inertia of reinforcing bars about the elastic neutral axis of the composite section, K is the effective length factor, L is the laterally unbraced length of the member, $L_c = KL$ = effective length of the member, $f_{c'}$ is the specified compressive strength of concrete.

3.2.2 EN 1994-1-1

As per EN 1994-1-1 the plastic resistance, P_P, of the cross section is the summation of its plastic resistance and is calculated from the below mentioned formula:

$$P_P = A_a F_Y + \alpha_C A_C (0.8 f_{CK}) + A_S f_{sk} \quad (16)$$

where A_a, A_c and A_s are the areas of the steel section, the concrete and the reinforcing steel respectively. f_y, f_{ck}, f_{sk} are the yield strengths of the steel section, the characteristic compressive strength of the reinforcing steel respectively, α_c strength coefficient for concrete, which is 1.0 for concrete filled tubular sections, 0.85 for encased and rectangular sections. For slender columns with low elastic critical load, overall buckling may be critical. Thus, increase in the slenderness will decrease the capacity of the column. EC4 has illustrated non-dimensional slenderness curves from which the capacity of the composite column can be estimated. The code also limits the depth-to-thickness ratio for local buckling avoidance in the section. $h/t \leq 50\varepsilon$ where $\varepsilon = \sqrt{\frac{250}{f_y}}$, f_y is the yield strength of the steel section in N/mm^2. The adopted slenderness satisfies the above-mentioned condition. The reduction in the capacity due to slenderness is taken care by non-dimensional slenderness ratio $\bar{\lambda}$. The reduced capacity, P, is calculated by $P = \chi P_P$ where χ is the reduction factor due to column buckling and is a function of the non-dimensional slenderness of the composite column.

AISC extends the design method of steel columns to CFT columns. The yield stress (f_y) of the steel tube and $0.85\ f_c$ of the in-filled concrete are used to determine the nominal axial load-carrying capacity, and then local buckling is considered based on the slenderness of the columns. EC4 considers the composite action between the filled concrete and the steel tube. The axial load-carrying capacity of the CFT columns is calculated by adding the contributions of the steel tube and the concrete core, and the increase in concrete strength caused by confinement is considered for the concrete core.

Table 5 gives a comparison of experimental and analytical results. The experimental results obtained are significantly higher than the results predicted by the methodology proposed in the codes. This indicates that the models used in these design codes do not accurately account for the composite action of these members. AISC extends the design method of steel columns to CFT columns. The yield stress

(f_y) of the steel tube and *0.85* f_c of the in-filled concrete are used to determine the nominal axial load carrying capacity, and then local buckling is considered based on the slenderness of the columns. EC4 considers the composite action between the filled concrete and the steel tube. The axial load-carrying capacity of the CFT columns is calculated by adding the contributions of the steel tube and the concrete core, and the increase in concrete strength caused by the confinement is considered for the concrete core. These expressions given in the code provisions are somewhat conservative, and they should be modified accordingly to get the full advantage of the composite behaviour.

Table 5: Comparison of experimental and analytical results of composite columns

Specimen	**KL/r**	**λ**	**Test (kN)**	**AISC 360-16 (kN)**	**EC4 (kN)**	**Test/AISC 360-16**	**Test/ EC4**
SNPC	15.301	0.022	413.3	356.05	344.12	1.16	1.20
INPC	45.904	0.193	396.7	321.72	309.94	1.23	1.28
LNPC	61.205	0.344	375.1	294.37	284.99	1.27	1.32
SPC	15.35	0.026	394.9	353.24	340.23	1.12	1.16
IPC	46.04	0.229	378.2	320.06	307.36	1.18	1.23
LPC	61.39	0.387	360.2	293.61	282.79	1.23	1.27
Mean						1.198	1.243
SD						0.055	0.058
CV%						4.583	4.680
β						3.48	3.63
λ is non-Dimensional slenderness ratio, KL/r is Effective Slenderness ratio, β is the reliability index, CV% is the coefficient of variation in percentage, SD is the Standard Deviation.							

4. Reliability analysis

Reliability analysis was performed to evaluate relative reliability of codal guidelines for performed tests. The analysis was performed as recommended in North American Specification for the design of cold formed steel structural members. The reliability index was calculated using the equation 17. The parameters M_m, F_m, V_m, V_f, were assumed as 1.10, 1.00, 0.10, and 0.05 respectively were determined by statistical analysis. P_m is the mean value included in the table 4 and 5. The coefficient of variation of test results were lower than the code specified value. Hence the minimum as specified in the code 0.065 was adopted. The coefficient of variation of load effect V_Q was taken as 0.21 for LRFD. The calibration coefficient (Cϕ) was taken as 1.52. As per NAS-2016, the correction factor (C_p) was taken as 5.7 since three specimens were tested for each variation. The resistance factor (ϕ) was taken as 0.85 as recommended in IS 800[18].

$$\beta = \frac{\ln\left(\frac{M_m F_m P_m C_\emptyset}{\phi}\right)}{\sqrt{V_P^2 + V_M^2 + V_F^2 + V_Q^2}} \tag{17}$$

The target reliability index was taken as 3.0. when the reliability of tested specimen was more than 3.0 indicates the occurrence highly reliable predicted value.

5. Numerical Modeling and Validation

A numerical modelling framework was developed in conjunction with the experimental data to conduct a parametric study. Finite element (FE) models were developed for each of the specimens tested experimentally. In this work, the commercial FE software package (ABAQUS) is employed to develop the computational models.

5.1 Parts and Meshing

The proposed FE model consists of two parts: steel tube and concrete. The self-tapping screws were not modelled since it was considered as a rigid continuous connection (similar to welding). The dominant deformation in the concrete core is compression without rotation. Hence 8-noded reduced integration brick elements with three degrees of freedom per node (C3D8R) would be the most effective element to reflect the concrete deformation characteristics [23]. 4-noded reduced integration shell elements (S4R) with six degrees of freedom per node have been used for the steel section [24]. After mesh convergence studies (Fig. 7), a mesh size of 10 mm was adopted, giving reliable results in minimum computational time. The geometry of the assembly was defined by creating instances of part and then positioning the instances relative to each other in a global coordinate system.

5.2 Loading and Boundary Conditions

A reference point (RP) was created at the centre of the end section; the steel and the concrete nodes were tied to this point using rigid body constraints as shown in Fig. 8. This constraint eliminates the need for endplates in the model, in this way the load and the boundary conditions were applied directly to this reference point. All the degrees of freedom except the displacement at the loaded end along the loading direction were restrained or simulating the pinned boundary condition.

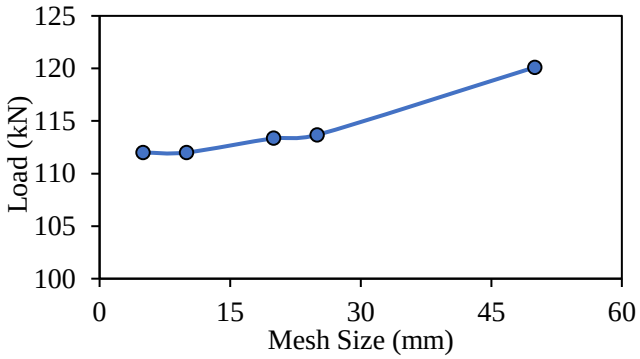

Fig. 7 Mesh convergence study results

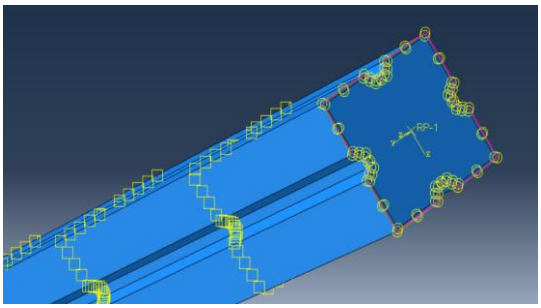

Fig. 8 Load and boundary conditions applied to RP

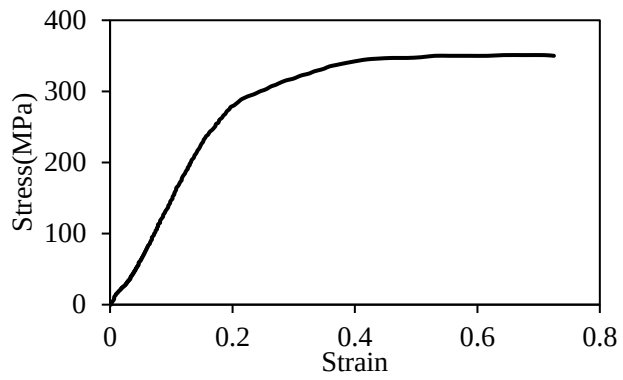

Fig. 9 Stress-Strain curve of steel

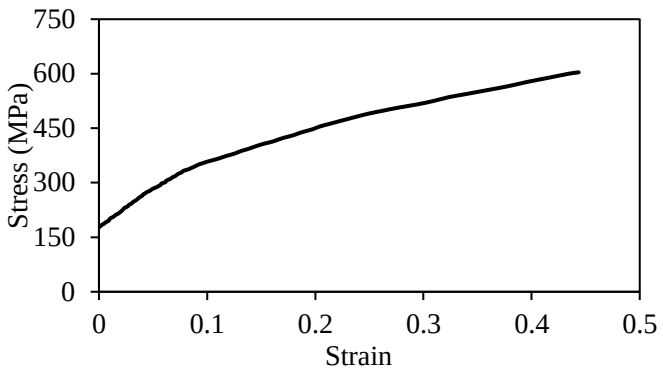

Fig. 10 Plastic stress-strain curve of steel

5.3 Material Properties

5.3.1 Steel Tube

An elastic-plastic stress-strain model was employed for the steel section. The material is considered isotropic and homogeneous. While defining the material property, the nominal stress and strain values are converted to true stress and logarithmic plastic strain using Eqs. (18) and (19).

$$\sigma_{true} = \sigma_{nom}(1 + \varepsilon_{nom}) \tag{18}$$

$$\varepsilon_p = \ln(1 + \varepsilon_{nom}) - \frac{\sigma_{true}}{E} \tag{19}$$

Where E is Young's modulus.

The plastic stress-strain curve provided in ABAQUS is shown in Fig. 10.

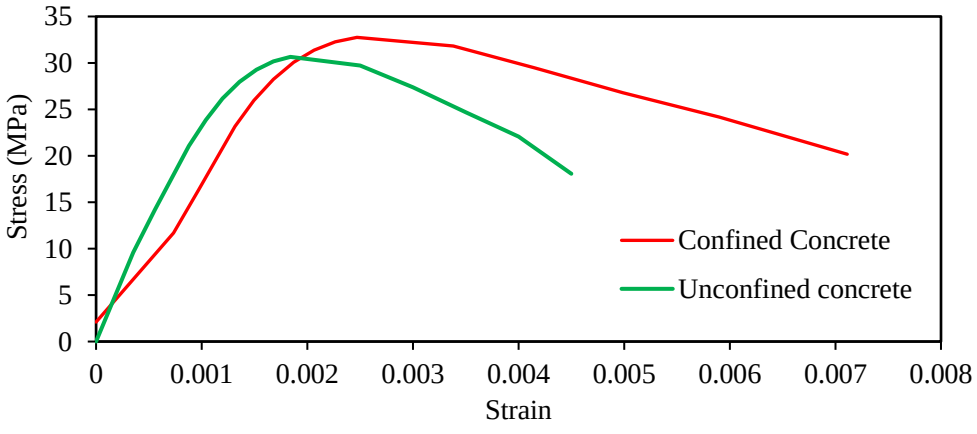

Fig. 11 (a) Equivalent Compressive Stress-Strain Diagram for Confined Concrete

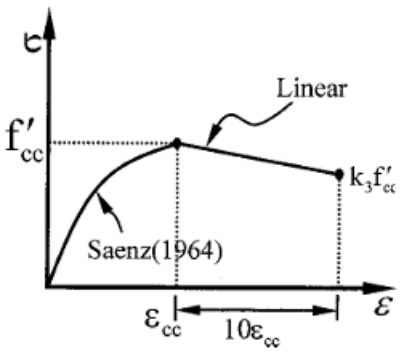

Fig. 11 (b) Uniaxial stress strain relation for concrete

5.3.2 Confined Concrete

The equivalent stress-strain diagram for confined concrete under compressive loading, as shown in Fig. 11, is used in the proposed FE model. This approach is similar to the one adopted by Ellobody and

Young [9]. The maximum concrete stress and corresponding strain were estimated by the following equations.

$$f'_{cc} = f'_c + k_1 f_1 \tag{20}$$

$$\varepsilon_{cc} = \varepsilon_c \left(1 + k_2 \frac{f_1}{f'_c}\right) \tag{21}$$

Where ec = strain corresponding to Fc' and was set as 0.3% and ff = confining pressure around the concrete core. Meanwhile, the constants k1 and k2 were set as 4.1 and 20.5 based on the studies of Richart et al. (1928).[25] The stress- strain relation up to (fcc, ecc) was defined by the following equation, which was a modification of saenz's (1964)[26].

$$\sigma = \frac{E_C \varepsilon}{1 + (R + R_e - 2)\left(\frac{\varepsilon}{\varepsilon_{cc}}\right) - (2R - 1)\left(\frac{\varepsilon}{\varepsilon_{cc}}\right)^2 + \left(\frac{\varepsilon}{\varepsilon_{cc}}\right)^3} \tag{22}$$

$$R = \frac{R_e(R_\sigma - 1)}{(R_\varepsilon - 1)^2} - \frac{1}{R_e} \tag{23}$$

$$R_e = \frac{E_c}{E_0} \tag{24}$$

$$E_0 = \frac{f'_{cc}}{\varepsilon_{cc}} \tag{24}$$

And R_σ and R_ε were set equal to 4 as suggested by Elwi and Murray (1979)[27]. The stress strain relationship after f'_{cc} , $\varepsilon_{cc}$was assumed to be linear, with k_3 defining the stiffness degradation.

The material parameters used in defining the nonlinear compressive behaviour of the concrete fill are given in Table 6. After establishing the uniaxial stress-strain diagram for confined concrete in both compression and tension, the concrete material behaviour can then be defined in ABAQUS as shown in Table 6.

Table 6 Concrete damage model parameters

Dilation Angle	Eccentricity	σ_{b0}/σ_{c0}	K	Viscosity Parameter
37.1	0.1	1.162	0.7255	0

5.4 Analysis

An Eigenvalue buckling analysis was first carried out from the linear perturbation step. In the nonlinear analysis, the stiffness matrix was updated periodically (for every iteration of every load increment) based on the current deformed shape of the structure. The stiffness may change from increment to increment due to P-Delta effects, large displacements and material non-linearity. The ultimate load capacity of the structure was also obtained from the analysis.

5.5 Initial Imperfections

The initial imperfection of the specimens was included in the load-deflection analysis using the *IMPERFECTION option available in ABAQUS. In this study, the shape of the initial local

imperfections was assumed as the first buckling mode shape obtained from the eigenvalue buckling analysis. The *CONTACT PAIR option is used to simulate the interaction between the concrete infill and steel walls. These surfaces were tied using a tie constraint option, and the buckling analysis was carried out. Thus, the eigenvalue analysis from this model was used to obtain the first buckling mode shape. The magnitude of the initial imperfection was taken as 0.006w (w width of the column) or the local buckling mode and L/1500 (L length of the column) for the global buckling mode proposed by Dubina et al. [28].

5.6 Contact Properties

The interaction between the steel and concrete was modelled using the *CONTACT PAIR option and surface-to-surface contact type. This contact requires a pair of surfaces named master and slave surfaces to be defined. To reduce numerical errors, the slave surface should belong to a softer material and have a finer mesh than the master one. Therefore, the outer surfaces of concrete were set as master surfaces whilst the inner surfaces of steel tubes were set as slave surfaces. The normal behaviour between the master and slave surfaces was simulated by the "hard" contact, which allows for separating the two surfaces after contact. The tangent behaviour between the two surfaces was simulated by the Coulomb friction model with a friction coefficient of 0.25 [29].

5.7 Comparison with Experimental Results

The numerical models developed were able to accurately predict the axial load behaviour of the columns in conjunction with the experimental results.

5.7.1 Hollow columns

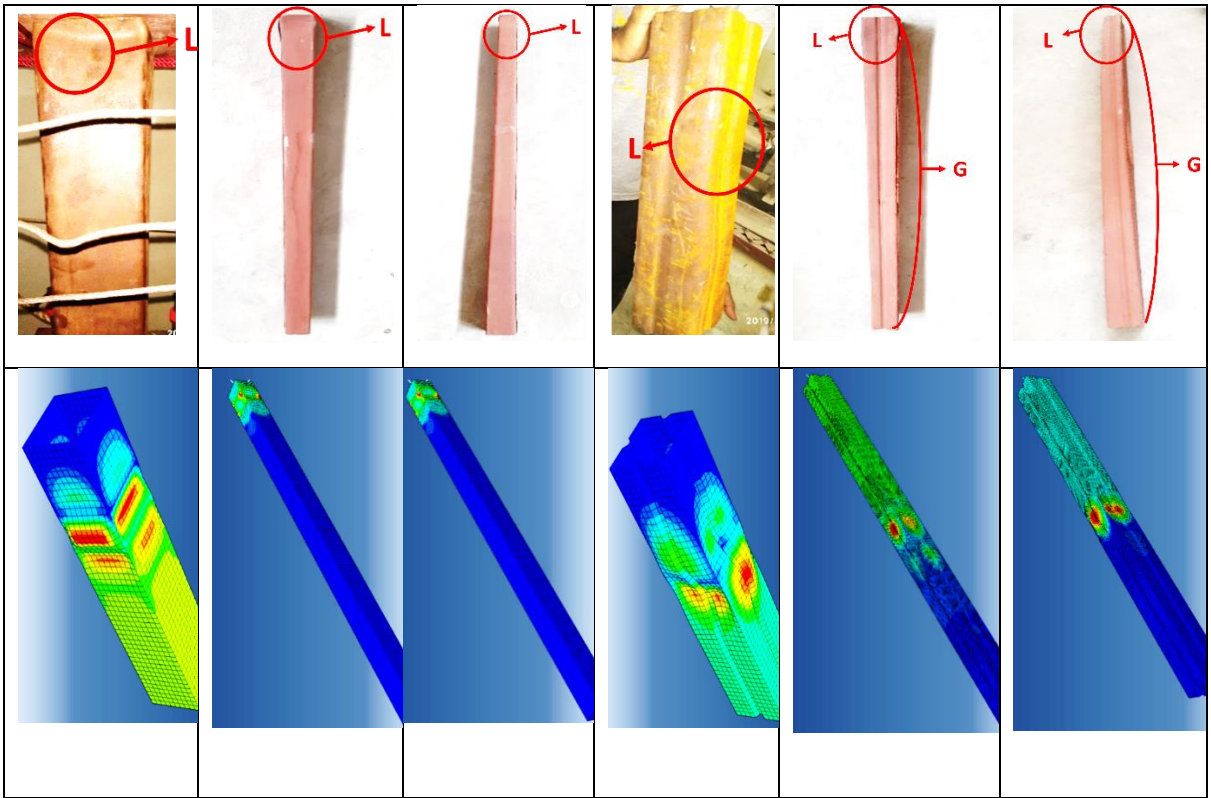

L & G are Local and Global buckling failures respectively

Fig. 12 Comparison of experimental and numerical behaviour of Hollow Plain Columns

Fig. 13 Comparison of experimental and numerical behaviour of Hollow Profiled Columns

The failure mode of columns observed during numerical analysis was also similar to that reported experimentally. For the plain sections, local buckling was observed in short, intermediate and long hollow plain columns (Fig 12). In Fig. 13, the stiffener in the profiled section changed the failure mode into a combination of local and global buckling. The inclusion of stiffeners increases the axial load carrying capacity of hollow sections. The load-displacement curves obtained from experimental and numerical analysis are compared, and a close agreement was observed (Figs. 14-16).

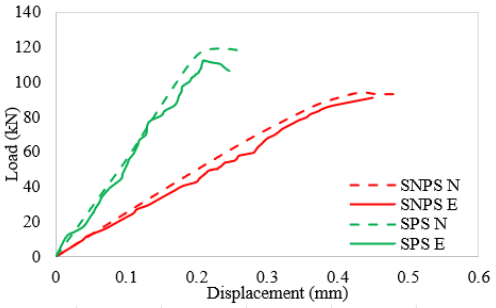

Fig. 14 Comparison of experimental and numerical behaviour of short hollow columns

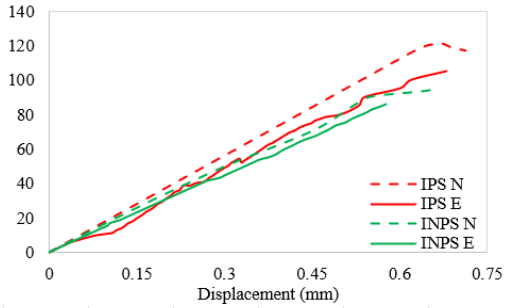

Fig. 15 Comparison of experimental and numerical behaviour of hollow intermediate columns

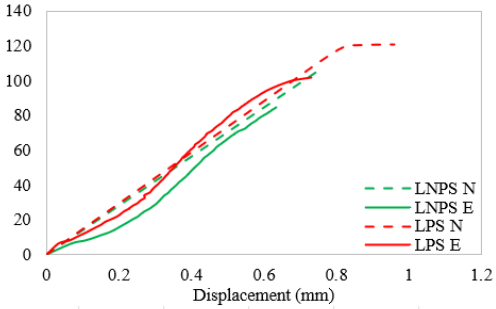

Fig. 16 Comparison of experimental and numerical behaviour of long hollow columns

5.7.2 Composite Columns

Fig. 19 and Fig. 20 compare the deformed shape predicted by the numerical analysis and the deformed shape obtained from experimental studies. The stress distribution on steel and concrete for plain and profiled sections are shown in Fig. 17 and 18. There is a non-uniform variation of stress in steel of plain section varying between 142MPa to 184MPa. This leads to local buckling of the steel in plain composite sections. However, due to the stiffeners, profiled sections developed uniform stress of 187MPa throughout the length and uniformed across the cross-section. As a result, a higher axial load was expected to be taken by the profiled section compared to the plain sections. The concrete in plain sections reached a stress value up to 33MPa. However, the stiffeners in the profiled column created regions of stress concentration near the edges, limiting the maximum stress that concrete could resist. The load taken by the concrete section was less in the case of profiled sections when compared to the plain section. Consequently, the total axial load taken by the profiled and plain composite columns was similar. The load-displacement curves are as in Figs. 21-23.

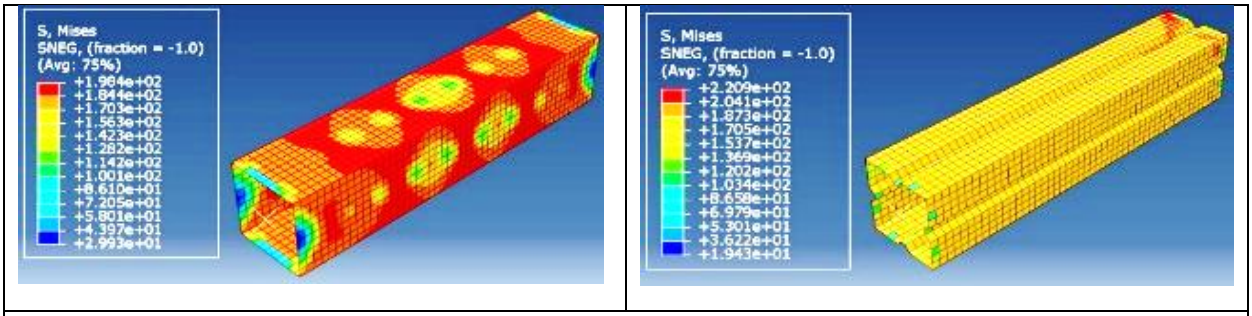

Fig. 17 Stress Distribution on Steel

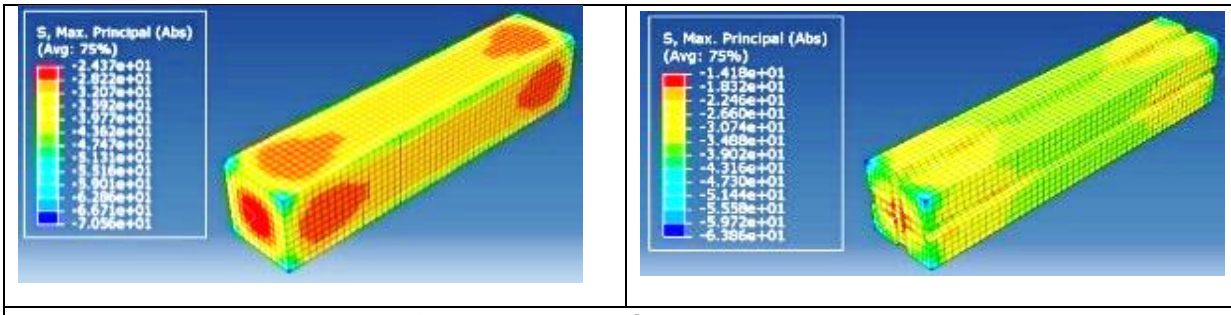

Fig. 18 Stress Distribution on concrete

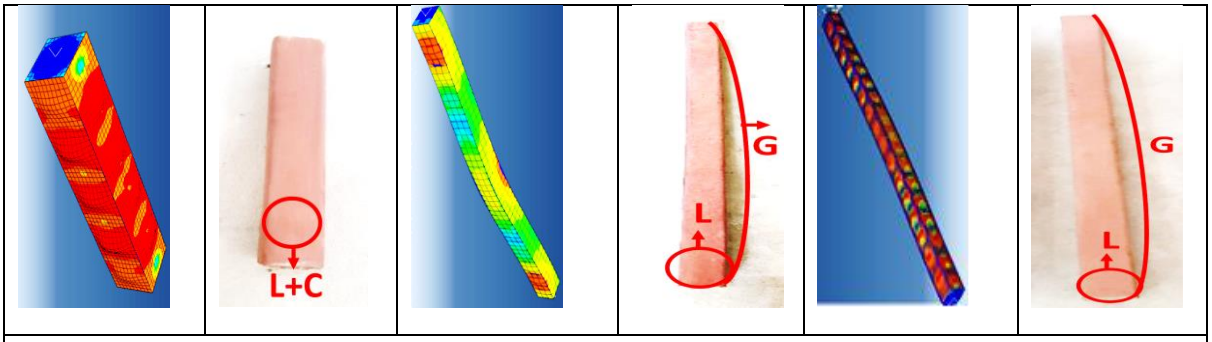

L, G & C are Local, Global buckling failures and Crushing of concrete respectively

Fig. 19 Comparison of experimental and numerical behaviour of Composite Plain Columns

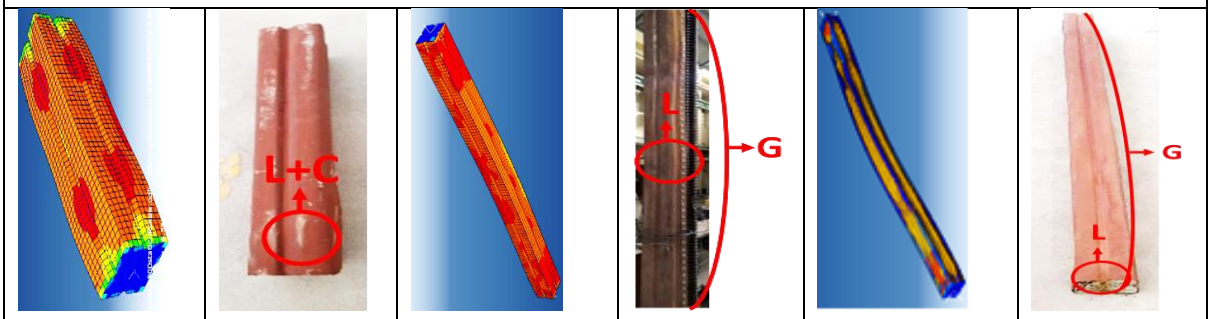

Fig. 20 Comparison of experimental and numerical behaviour of Composite Profiled Columns

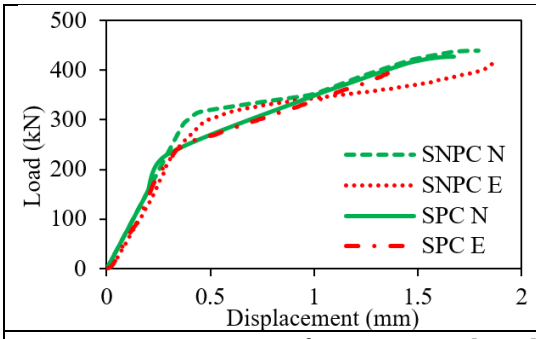

Fig. 21 Comparison of experimental and numerical behaviour of short composite columns

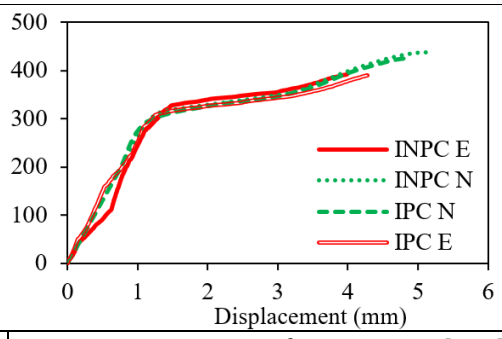

Fig. 22 Comparison of experimental and numerical behaviour of composite intermediate columns

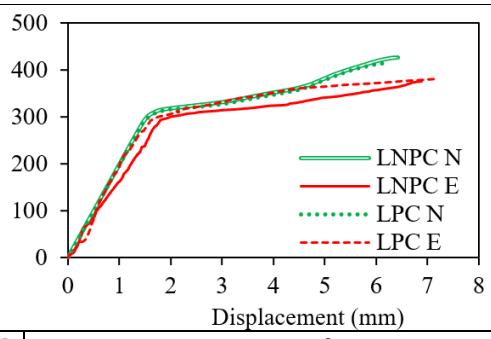

Fig. 23 Comparison of experimental and numerical behaviour of long composite columns

5.7.3 Strength Index

A parameter called Strength Index (SI) [11] is used to evaluate the effect of different parameters on the load-bearing capacity of composite columns.

$$SI = \frac{N_{ue}}{F_c A_c + f_y A_s} \tag{25}$$

Where f_c is the characteristic compressive strength of concrete, A_c is the concrete area, A_s is the area of steel, and f_y is the yield strength of steel tube.

The bar chart in Fig. 24 depicts the SI values of the columns analysed.

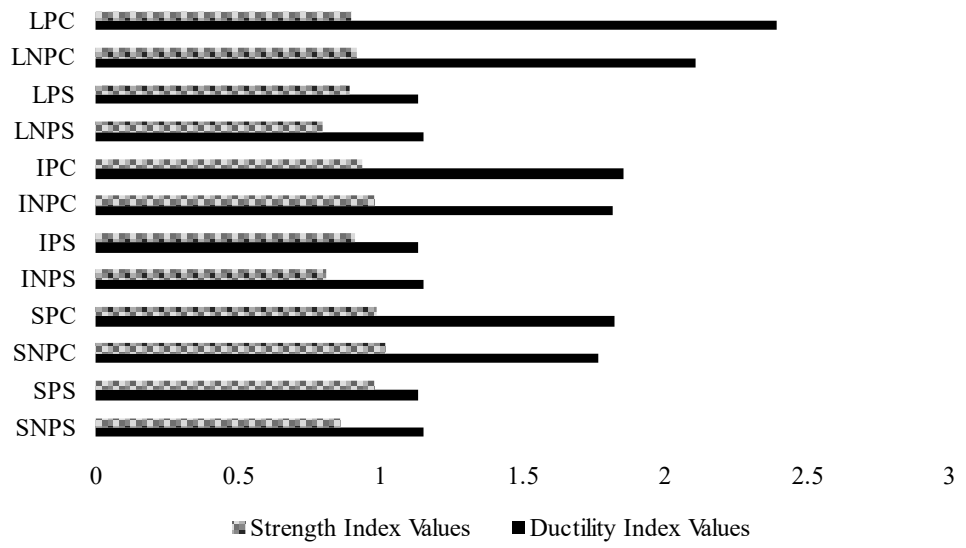

Fig. 24 Strength Index (SI) values and Ductility Index (DI) values

The profiled section's SI values were much higher than the SI values of the plain section in the case of CFS hollow columns. However, plain and profiled composite sections have almost equal SI values indicating that profile does not improve the axial load capacity of composite columns as it does in hollow columns.

5.7.4 Ductility Index

To evaluate the effect of different parameters on the ductility of composite columns, a parameter called Ductility Index (DI) [13] is computed.

$$\mathrm{DI} = \frac{\varepsilon_{85}}{\varepsilon_y} \tag{26}$$

Where ε_{85} is the axial strain when the load falls to 85% of the ultimate load and ε_y is the axial strain when the load attains 75% of the ultimate load in the pre-peak stage.

DI values of all the sections analysed can be inferred from Fig. 24.

The DI values of both plain and profiled hollow sections indicate that profiles do not influence the ductility behaviour of CFS hollow sections. However, composite profiled sections show improved ductility when compared to the plain sections.

6. Parametric Study

The literature commented on the improved axial behaviour of CFS columns with an increase in the stiffener angle, stiffener dimensions and stiffener numbers [12], [30]. Parametric studies were carried out to assess the effect of the stiffener angles, sizes, and stiffeners on composite columns. The details of the models adopted for numerical analysis are given in Table 7. Nomenclature CM is used for the profiled control model with a 120.96^0 angle. For the other models, the first number indicates the number of stiffeners. The letter S stands for stiffener. The last number denotes the model number in that category, H stands for hollow sections and the letter C stands for the composite column.

Short columns with stiffeners of angle 120.96^0, 90.0^0 and 141.76^0 (CM, 1S1, 1S2) were analysed to compare the effect of stiffener angles. For the hollow sections, axial strength was found to increase slightly with the increase in the stiffener angle. In contrast, reduction in stiffener angle did not seem to influence much, as can be seen from Table 7. The SI against Strain curve in Figs. 25-27 indicate that the profiles with an inclination angle greater than the control model exhibited improved ductility in the case of CFS hollow columns. However, all composite sections showed similar behaviours irrespective of the stiffener angle.

A few models with varying stiffener width and depth 1S1, 1S3, 1S4 were analysed to study the influence of dimensions of the stiffeners on the axial behaviour of columns. A slight increase in SI can be noted in 1S3 and 1S4. There is a noticeable increase in the ductility of CFS hollow columns with the increase in depth and width of the stiffener. Irrespective of the stiffener dimensions, all composite columns exhibited similar behaviours (Fig. 26).

The effect of the number of stiffeners on the axial behaviour of the hollow and composite columns was analysed by comparing CM with 2S1 and 1S1 with 2S2. There was no considerable improvement in the axial capacity of the columns with an increase in the number of stiffeners. However, a slight improvement in ductility was observed in both hollow and composite two stiffener models (Fig. 27). It is found that the axial load carrying capacity of the columns is independent of the number of stiffeners provided in the steel section.

Table 7: Details of models for parametric study

Model	**Cross-section**	**Stiffener specifications**	**Section Type**	**Axial capacity Analytical (kN)**	**Axial capacity Numerical (kN)**	**Strength Index (SI)**
CM		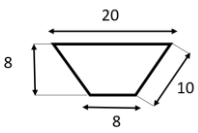	Hollow (CMH)	114.048	121.22	1.063
Angle $=120.96^0$			Composite (CMC)	400.61	427.42	1.067
1S1			Hollow (1S1H)	122.50	130.32	1.063

Angle =90^0		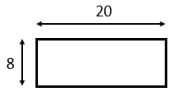	Composite (1S1C)	403.30	430.40	1.067
1S2 Angle =141.76^0	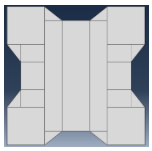	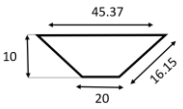	Hollow (1S2H)	112.91	122.94	1.088
			Composite (1S2C)	373.70	400.45	1.072
1S3 Angle =90^0	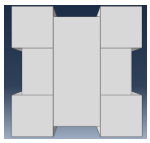	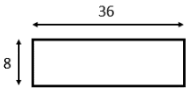	Hollow (1S3H)	122.50	131.97	1.077
			Composite (1S3C)	387.94	414.38	1.068
1S4 Angle =90^0		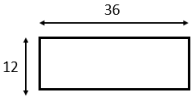	Hollow (1S4H)	130.94	142.09	1.085
			Composite (1S4C)	379.104	403.78	1.065
2S1 Angle = 120.96^0	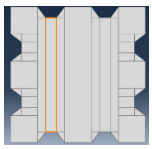	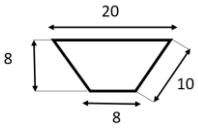	Hollow (2S1H)	122.50	130.43	1.065
			Composite (2S1C)	395.62	424.32	1.072
2S2 Angle = 90^0	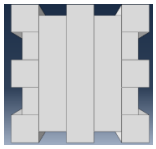	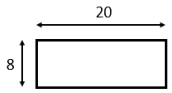	Hollow (2S2H)	139.39	149.77	1.075
			Composite (2S2C)	400.99	428.79	1.069

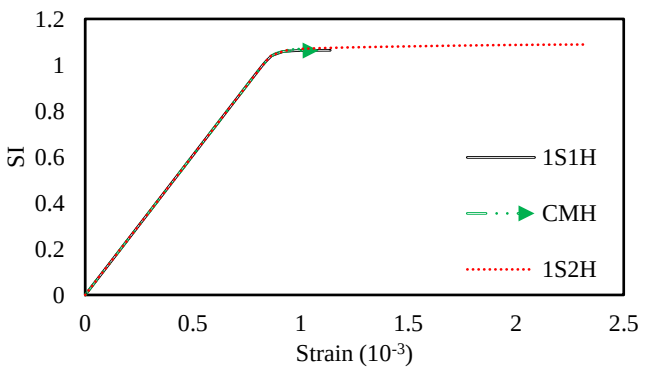

(a) Hollow column

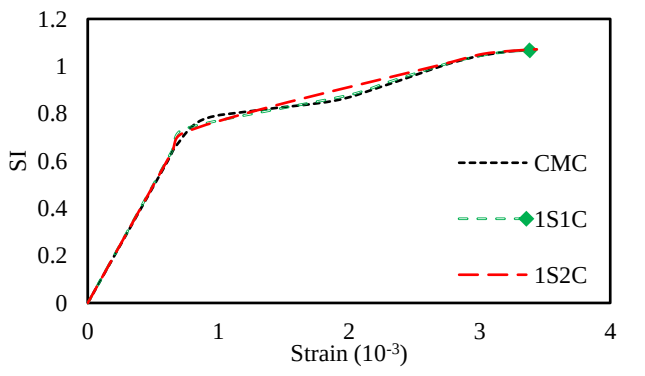

(b) Composite column

Fig. 25 SI vs Strain curve of columns with varying stiffener angles

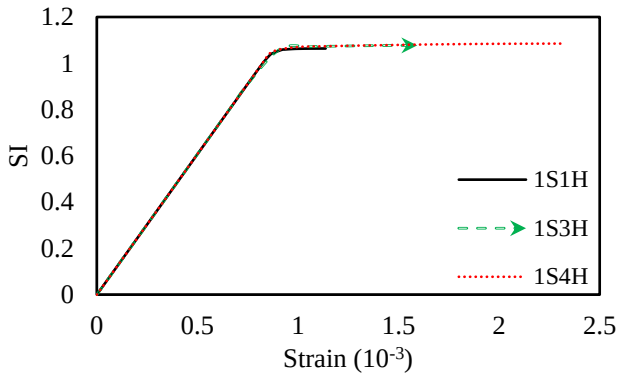

(a) Hollow column

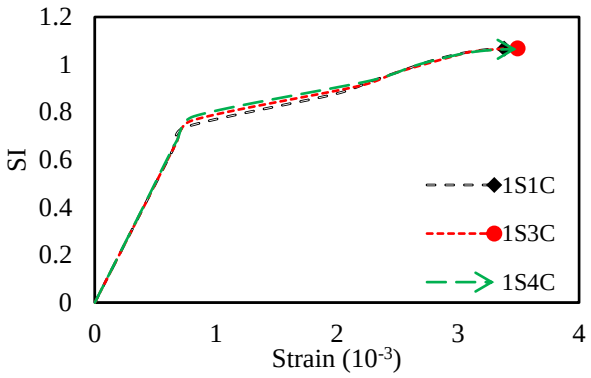

(b) Composite column

Fig. 26 SI vs Strain curve of columns with varying stiffener dimensions

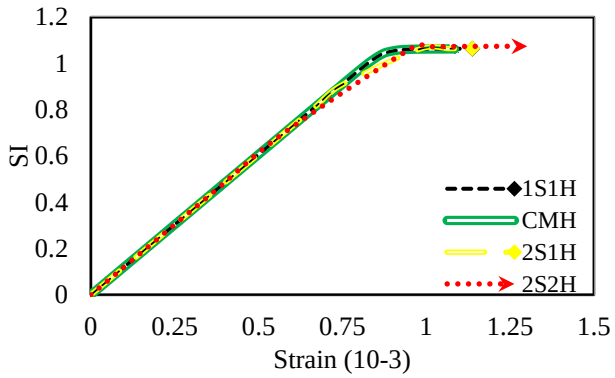

(a) Hollow column

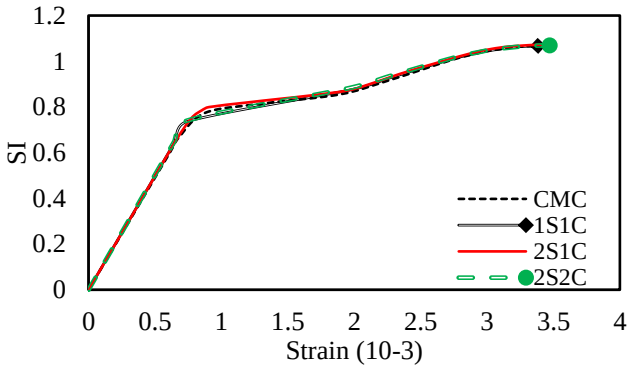

(b) Composite column

Fig. 27 SI vs Strain curve of columns with varying stiffener number

7. Buckling Curve

7.1 Buckling curve from numerical studies

The parametric study was extended to a wide range of slenderness range for the length of the column varying between 500mm to 5000mm. The reduction factor for buckling, χ (P/P_y), is plotted against the non-dimensional slenderness ratio, λ as shown in Fig. 28.

The non-dimensional slenderness ratio is evaluated as:

$$\lambda = \sqrt{\frac{P_y}{P_e}} \tag{27}$$

Where P_y is the plastic resistance of the section,

$$P_{no} = F_y A_s + f_c' A_c \tag{28}$$

$$P_e = \frac{\pi^2 (EI_{eff})}{{L_c}^2} \tag{29}$$

$$EI_{eff} = E_s I_s + E_c I_c \tag{30}$$

P_e is the elastic buckling load, EI_{eff} is the effective stiffness of composite section.

Profiled composite columns gave higher values of buckling reduction factor in most slenderness ranges, indicating that the profiled sections are more effective.

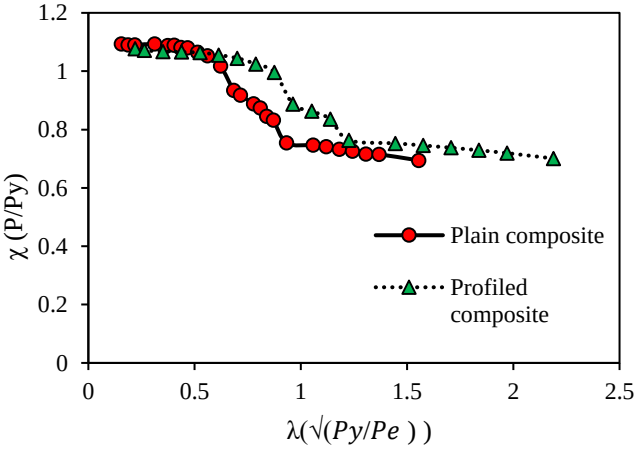

Fig. 28 Buckling Curve of Plain and Profiled Composite Column

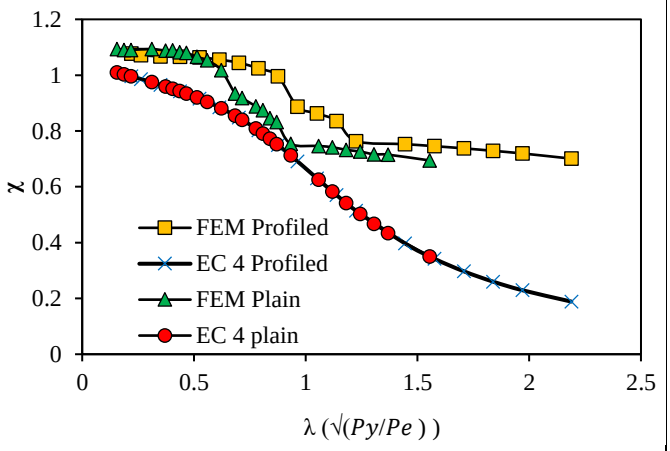

Fig. 29 Comparison of Numerical and EC4 Buckling Curves

The columns with slenderness up to 0.62 in the case of plain and 0.87 in the case of profiled sections failed but crushing and bulging out of concrete, while columns in the slenderness range 0.62 – 0.87 for plain sections and 0.87 – 1.23 for profiled sections exhibited a combination of crushing of concrete and global buckling. Columns longer than this range failed by pure buckling. This is depicted in Fig. 30.

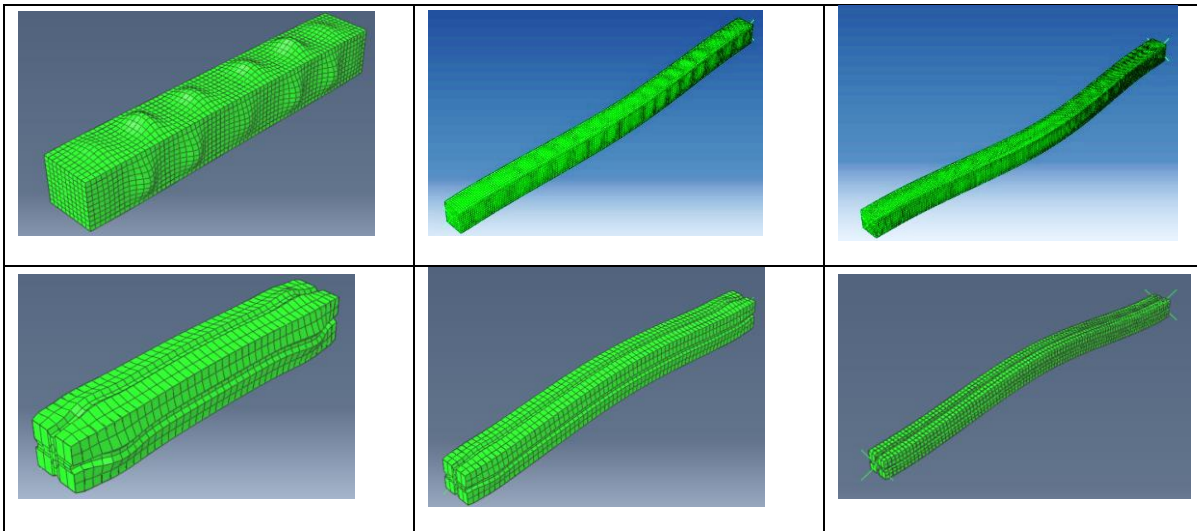

(a) Failure by crushing and bulging out of concrete

(b) Failure by the combination of crushing of concrete and global buckling

(c) Failure by global buckling

Fig. 30 Failure behaviour of columns belonging to various slenderness range

7.2 Comparison with EC4

A reduction factor χ is considered to evaluate the maximum column compressive strength as per EN 1994-1-1[31]. The reduction factor is evaluated as follows:

$$\chi = \frac{1}{\phi + [\phi^2 - \lambda^2]^{0.5}} \tag{31}$$

$$\varphi = 0.5[1 + \alpha(\lambda - 0.2)] + \lambda^2 \tag{32}$$

Where α is the imperfection factor, considered equal to 0.21 (curve a).

Fig. 29 compares the buckling curve obtained from the FE analyses and based on the design strength predicted by EC4 for plain and profiled columns, respectively. From Fig. 29, the buckling reduction factor, χ, obtained from numerical investigations showed higher values when compared to the Eurocode recommendations. It is suggested to conduct a more extensive parametric analysis, in order to propose an alternative buckling curve for both plain and profiled CFS-concrete composite columns that give less conservative value and a more economical design.

8. Concluding Remarks

Composite cold-formed steel-concrete columns (CFSCs) exhibit improved strength and ductility characteristics while the introduction of web stiffeners can further enhance their buckling performance. The cold-formed steel tube sections employed in this study were formed using self-tapping screws, a technique which is prevalent is several developed countries.

This study focuses on the effect of stiffeners on the concentric axial load behaviour of composite cold-formed steel-concrete columns with self-tapping screws. An experimental campaign and parametric studies were carried out to understand the influence of various geometric parameters of the stiffeners on the composite behaviour of CFS-concrete composite columns. Buckling curves were developed for plain and profiled composite sections by extending the numerical study to various slenderness ratios.

Following, the conclusions are synopsized below:

1. Composite columns have almost four times the load-carrying capacity of bare steel hollow columns.
2. Self-tapping screws provide a good type of (continuous) connection in CFS tubular columns.
3. Stiffeners are found to delay local buckling in the case of hollow columns effectively. There was a significant increase in the load-carrying capacity.
4. The use of stiffeners creates many regions of stress concentration on the concrete face. This limits concrete from reaching the maximum stress. Hence, the profiled columns were found to have an axial load capacity almost equal to those of their plain counter ones, hence separate design guidelines are not necessary.
5. The ductility of CFS hollow columns was found to improve with the increase in the angle of stiffener, depth and width of stiffener as well as the number of stiffeners, though their axial capacity was observed to be the same.
6. Variation of parameters associated with stiffeners showed very little or no influence on the axial load capacity of the CFS-concrete composite columns.
7. The buckling reduction factor of profiled composite columns showed higher values in the majority of the slenderness indicating the profile's effectiveness when compared to plain.

This study is aimed to be extended to intermediate and long composite columns. The effect of eccentric load on the composite columns with stiffeners should also be investigated. Comprehensive parametric studies are required to be carried out to propose updated buckling curves for both plain and profiled CFS-concrete composite columns.

References

[1] N. . Shanmugam and B. Lakshmi, "State of the art report on steel-concrete composite columns," *J. Constr. Steel Res.*, vol. 57, no. 10, pp. 1041–1080, 2001.

[2] L. H. Han, W. Li, and R. Bjorhovde, "Developments and advanced applications of concrete-filled steel tubular (CFST) structures: Members," *J. Constr. Steel Res.*, vol. 100, pp. 211–228, 2014, doi: 10.1016/j.jcsr.2014.04.016.

[3] X. L. Zhao, L. H. Han, and H. Lu, "Concrete-filled Tubular Member," *1st Ed. Spon Press. Oxon.*, 2010.

[4] R. Rahnavard, H. D. Craveiro, M. Lopes, R. A. Simões, L. Laím, and C. Rebelo, "Concrete-filled cold-formed steel (CF-CFS) built-up columns under compression: Test and design," *Thin-Walled Struct.*, vol. 179, no. May, p. 109603, 2022, doi: 10.1016/j.tws.2022.109603.

[5] B. Evirgen, A. Tuncan, and K. Taskin, "Structural behavior of concrete filled steel tubular sections (CFT/CFSt) under axial compression," *Thin-Walled Struct.*, vol. 80, pp. 46–56, 2014, doi: 10.1016/j.tws.2014.02.022.

[6] B. Uy, "Strength of Concrete Filled Steel Box Columns Incorporating Local Buckling," *J. Struct. Eng.*, vol. 126, no. 3, pp. 341–352, 2000, doi: 10.1061/(asce)0733-9445(2000)126:3(341).

[7] Q. X. Ren, L. H. Han, D. Lam, and C. Hou, "Experiments on special-shaped CFST stub columns under axial compression," *J. Constr. Steel Res.*, vol. 98, pp. 123–133, 2014, doi: 10.1016/j.jcsr.2014.03.002.

[8] Z. He and X. Zhou, "Strength design curves and an effective width formula for cold-formed steel columns with distortional buckling," *Thin-Walled Struct.*, vol. 79, pp. 62–70, 2014, doi: 10.1016/j.tws.2014.02.004.

[9] H. B. Ge and T. Usami, "Strength analysis of concrete-filled thin-walled steel box columns," *J. Constr. Steel Res.*, vol. 30, no. 3, pp. 259–281, 1994, doi: 10.1016/0143-974X(94)90003-5.

[10] C.S.Huang *et al.*, "Axial load behaviour of stiffened concrete filled steel columns," *J. Struct. Eng.*, no. 7, pp. 593–598, 2002, doi: 10.1093/jat/28.7.593.

[11] Z. Tao, L. H. Han, and Z. Bin Wang, "Experimental behaviour of stiffened concrete-filled thin-walled hollow steel structural (HSS) stub columns," *J. Constr. Steel Res.*, vol. 61, no. 7, pp. 962–983, 2005, doi: 10.1016/j.jcsr.2004.12.003.

[12] M. Nassirnia, A. Heidarpour, X. L. Zhao, and J. Minkkinen, "Innovative hollow corrugated columns: A fundamental study," *Eng. Struct.*, vol. 94, pp. 43–53, 2015, doi: 10.1016/j.engstruct.2015.03.028.

[13] Z. Tao, L. H. Han, and D. Y. Wang, "Strength and ductility of stiffened thin-walled hollow steel structural stub columns filled with concrete," *Thin-Walled Struct.*, vol. 46, no. 10, pp. 1113–1128, 2008, doi: 10.1016/j.tws.2008.01.007.

[14] AISC (American Institute of Steel Construction), "Specification for Structural Steel Buildings, ANSI / AISC 360-16," *Am. Inst. Steel Constr.*, p. 676, 2016.

[15] K. Rajmohan and A. S. Kumar, “Experimental investigation and prediction of optimum process parameters of micro-wire-cut EDM of 2205 DSS,” 2016, doi: 10.1007/s00170-016-8615-3.

[16] *IS 516 (1959): Method of Tests for Strength of Concrete*. .

[17] *IS 10262:2019, Concrete Mix Proportioning guideline, BIS, New Delhi*. .

[18] I. IS 800, *IS 800-2007 GENERAL CONSTRUCTION IN STEEL — CODE OF PRACTICE (Third Revision)*, no. December. 2007.

[19] J. Shen and M. A. Wadee, “Length effects on interactive buckling in thin-walled rectangular hollow section struts,” *Thin-Walled Struct.*, vol. 128, no. July, pp. 152–170, 2018, doi: 10.1016/j.tws.2017.04.006.

[20] *BS 5950-5:1998: Code of practice for design of cold-formed thin gauge sections.* .

[21] *AISI S100-16: North American Specification for the Design of Cold-Formed Steel Structural Members*. .

[22] IS 11384 (1985), “code of practice for composite construction in structural steel and concrete (CED 38: Special structures),” 1985.

[23] H. T. Thai, B. Uy, M. Khan, Z. Tao, and F. Mashiri, “Numerical modelling of concrete-filled steel box columns incorporating high strength materials,” *J. Constr. Steel Res.*, vol. 102, pp. 256–265, 2014, doi: 10.1016/j.jcsr.2014.07.014.

[24] E. Ellobody and B. Young, “Structural performance of cold-formed high strength stainless steel columns,” *J. Constr. Steel Res.*, vol. 61, no. 12, pp. 1631–1649, 2005, doi: 10.1016/j.jcsr.2005.05.001.

[25] R. L. Richart, Frank Erwin; Brandtzæg, Anton; Brown, “A study of the failure of concrete under combined compressive stresses,” *Univ. Illinois. Eng. Exp. Station. Bull.*, vol. 26, p. 12, 1928, [Online]. Available: https://www.ideals.illinois.edu/handle/2142/4277.

[26] Saenz. and L. P., “Equation for the stress-strain curve of concrete,” *ACI J.*, vol. 9, no. 61, pp. 1229–1235, 1964.

[27] A. A. Elwi and D. W. Murray, “a 3D Hypoelastic Concrete Constitutive Relationship,” *ASCE J Eng Mech Div*, vol. 105, no. 4, pp. 623–641, 1979, doi: 10.1061/jmcea3.0002510.

[28] D. Dubina and V. Ungureanu, “Effect of imperfections on numerical simulation of instability behaviour of cold-formed steel members,” *Thin-Walled Struct.*, vol. 40, no. 3, pp. 239–262, 2002, doi: 10.1016/S0263-8231(01)00046-5.

[29] X. Dai and D. Lam, “Numerical modelling of the axial compressive behaviour of short concrete-filled elliptical steel columns,” *J. Constr. Steel Res.*, vol. 66, no. 7, pp. 931–942, 2010, doi: 10.1016/j.jcsr.2010.02.003.

[30] M. Farahi, A. Heidarpour, X. L. Zhao, and R. Al-Mahaidi, “Compressive behaviour of concrete-filled double-skin sections consisting of corrugated plates,” *Eng. Struct.*, vol. 111, pp. 467–477, 2016, doi: 10.1016/j.engstruct.2015.12.012.

[31] *EN 1994-1-1, Eurocode 4: Design of composite steel and concrete structures, Part 1-1: General rules and rules for buildings, CEN, 2005*. .

Data Availability: The data used to support the findings of this study are available from the corresponding author upon request.

Funding Statement: The research and publication have no funding.